AJNR

This information is current as of August 12, 2025.

High Spatiotemporal Resolution 4D Flow MRI of Intracranial Aneurysms at 7T in 10 Minutes

L.M. Gottwald, J. Töger, K. Markenroth Bloch, E.S. Peper, B.F. Coolen, G.J. Strijkers, P. van Ooij and A.J. Nederveen

High Spatiotemporal Resolution 4D Flow MRI of Intracranial Aneurysms at 7T in 10 Minutes

L.M. Gottwald, J. Töger, K. Markenroth Bloch, E.S. Peper, B.F. Coolen, G.J. Strijkers, P. van Ooij, and A.J. Nederveen

ABSTRACT

BACKGROUND AND PURPOSE: Patients with intracranial aneurysms may benefit from 4D flow MR imaging because the derived wall shear stress is considered a useful marker for risk assessment and growth of aneurysms. However, long scan times limit the clinical implementation of 4D flow MR imaging. Therefore, this study aimed to investigate whether highly accelerated, high resolution, 4D flow MR imaging at 7T provides reliable quantitative blood flow values in intracranial arteries and aneurysms.

MATERIALS AND METHODS: We used pseudospiral Cartesian undersampling with compressed sensing reconstruction to achieve high spatiotemporal resolution (0.5 mm isotropic, ~30 ms) in a scan time of 10 minutes. We analyzed the repeatability of accelerated 4D flow scans and compared flow rates, stroke volume, and the pulsatility index with 2D flow and conventional 4D flow MR imaging in a flow phantom and 15 healthy subjects. Additionally, accelerated 4D flow MR imaging with high spatiotemporal resolution was acquired in 5 patients with aneurysms to derive wall shear stress.

RESULTS: Flow-rate bias compared with 2D flow was lower for accelerated than for conventional 4D flow MR imaging (0.31 ± 0.13, $P = .22$, versus 0.79 ± 0.17 mL/s, $P < .01$). Pulsatility index bias gave similar results. Stroke volume bias showed no difference for accelerated as well as for conventional 4D flow compared to 2D flow MR imaging. Repeatability for accelerated 4D flow was similar to that of 2D flow MR imaging. Increased temporal resolution for wall shear stress measurements in 5 intracranial aneurysms did not show a consistent effect for the wall shear stress but did show an effect for the oscillatory shear index.

CONCLUSIONS: Highly accelerated high spatiotemporal resolution 4D flow MR imaging at 7T in intracranial arteries and aneurysms provides repeatable and accurate quantitative flow values. Flow rate accuracy is significantly increased compared with conventional 4D flow scans.

ABBREVIATIONS: CS = compressed sensing; N_{card} = number of reconstructed cardiac timeframes; OSI = oscillatory shear index; PROUD = PROspective Undersampling in multiple Dimensions; R = acceleration factor; SENSE = sensitivity encoding; UIA = unruptured intracranial aneurysm; WSS = wall shear stress; WSS_{PS} = peak systolic WSS; WSS_{TA} = time-averaged WSS

Intracranial aneurysms can threaten a patient's life because of the risk of rupture followed by hemorrhagic stroke, which is associated with high morbidity and mortality.[1,2] Therefore, intracranial aneurysms need to be monitored regularly to assess whether they remain stable and asymptomatic or grow, with an increased risk of rupture. Treatment choices range from medical follow-up for stable aneurysms to coiling or clipping for growing aneurysms when the risk of rupture is considered too high.[1,2] For patients with unruptured intracranial aneurysms (UIAs) that

need long-term follow-up and who have no contraindications for MR imaging, it is advised to consider MR imaging rather than CTA.[2] Typical MR imaging examinations use TOF or gadolinium contrast to visualize the aneurysms; however, advanced 4D flow MR imaging sequences can additionally visualize and quantify complex blood flow patterns in the aneurysm.[3]

Please address correspondence to Lukas M. Gottwald, MSc, Department of Radiology and Nuclear Medicine, Amsterdam University Medical Centers, location AMC, University of Amsterdam, Meibergdreef 9, 1105 AZ Amsterdam, the Netherlands; e-mail: lukas.gottwald@outlook.com

Indicates open access to non-subscribers at www.ajnr.org

Indicates article with supplemental on-line table.

Indicates article with supplemental on-line photos.

Indicates article with supplemental on-line video.

http://dx.doi.org/10.3174/ajnr.A6603

In addition to measurements of basic blood flow volumes and velocities, 4D flow MR imaging allows the estimation of hemodynamic biomarkers, including wall shear stress (WSS).[4,5] Those have generated interest because abnormal WSS might be an indicator for aneurysm growth.[6,7] Moreover, it has been shown that the aneurysm wall is thin in regions of high WSS and vice versa.[8,9] This finding suggests that 4D flow MR imaging can provide added value in the clinical assessment of aneurysms. However, the implementation of 4D flow MR imaging in routine clinical practice has been hampered by long scan times required to achieve sufficient spatiotemporal resolution to image the complex blood flow patterns in the aneurysm.

A way to improve 4D flow MR imaging of intracranial aneurysms is the use of 7T MR imaging. The increased SNR compared with 3T can be exploited to obtain increased spatiotemporal resolution and/or reduced scan times.[10] High spatiotemporal resolution is desirable because it has been shown that hemodynamic parameters such as mean flow, peak flow, flow waveform, WSS, and oscillatory shear index[11] (OSI) are influenced by spatial and temporal resolution of 4D flow MR imaging measurements.[12] A rule of thumb is that, to be clinically acceptable, the scan time should not exceed 10 minutes[13] to fit into the clinical workflow and for patient comfort. Advanced accelerated 4D flow MR imaging techniques using pseudospiral Cartesian sampling with compressed sensing[14] (CS) can be used to achieve such short scan times. These techniques have already proved effective to accelerate 4D flow MR imaging of the aorta and carotid arteries.[15,16] While we believe such a method could also be beneficial for intracranial 4D flow acquisitions at 7T, this benefit has not been thoroughly validated so far.

Therefore, the aim of this study was to investigate whether highly accelerated, high resolution 7T 4D flow MR imaging can provide reliable quantitative blood flow values in intracranial arteries. Specifically, we investigated flow accuracy in a flow phantom as well as healthy subjects. Furthermore, we aimed to explore the use of this accelerated sequence for deriving WSS in patients with unruptured intracranial aneurysms.

MATERIALS AND METHODS

Undersampled 4D flow MR Imaging Acquisition and CS Reconstruction

Accelerated 4D flow MR imaging was acquired on two similar 7T systems (Achieva 7T; Philips Healthcare), one located at the National 7T Facility, Lund, Sweden, and one at the Spinoza Center for Neuroimaging, Royal Netherlands Academy of Arts and Sciences, Amsterdam, the Netherlands. The scanners were equipped with a 32-channel receive head coil (2TX/32RX; NovaMedical) and an in-house-developed software modification called (PROspective Undersampling in multiple Dimensions [PROUD]), which enables a pseudospiral k_y/k_z-plane acquisition scheme designed for incoherent undersampling with a variable sampling density.[15,16] The acquisition was performed continuously without cardiac triggering. The signal of a peripheral pulse transducer was stored with the k-space data and used for retrospective binning in different cardiac timeframes. Due to physiologic heart rate variability, the resulting k-t space was randomly filled, which is favorable for CS reconstruction and enabled retrospective changes of the temporal resolution.[16]

Reconstructions were performed off-line in Matlab R2016a (MathWorks) using MRecon (GyroTools) in combination with the Berkeley Advanced Reconstruction Toolbox (https://mrirecon.github.io/bart/).[17] A nonlinear parallel imaging and CS reconstruction were performed using a total variation sparsifying operator in time as previously described.[16]

Flow Phantom

A flow phantom was constructed, consisting of two merging plastic tubes surrounded by water (On-line Fig 1). Table salt (~20 g/L) was added to the water to improve B_1 field homogeneity. The inlets were connected to a custom-made MR imaging–compatible mechanical pulsatile pump placed on the scanner table. A linear actuator, in the form of a servo motor (CM2-X-56B20A; MUSCLE CORPORATION) coupled to a ball screw actuator (VLACT55-12-0150; THK CO., LTD.), was used to produce a pulsatile flow (peak flow rate, 2 mL/s; pump output, 0.175 L/min; heart rate, 57 beats per minute). The pump software provided a trigger signal to the MR imaging system for retrospective binning. The flow phantom was scanned at the National 7T Facility, Lund, Sweden.

At both inlets as well as the outlet, 2D flow MR imaging was acquired and considered as a reference (spatial resolution, 0.3 × 0.3 × 3.0 mm³; temporal resolution, 26.0 ms). The 2D flow scans were performed at the beginning and end of the experiment to verify flow stability. Two 4D flow scans were obtained with sensitivity encoding (SENSE) with an acceleration factor R = 3 (spatial resolution, 0.5 mm isotropic; temporal resolution, 65.8–87.7 ms). Moreover, six PROUD 4D flow scans were obtained with nominal acceleration factors of R = 4, 8, 12, 16, 32 (spatial resolution, 0.5 mm isotropic). These scans were reconstructed in 15 different combinations of effective acceleration factors and number of cardiac frames (N_{card}) (temporal resolution, 26.3–87.7 ms). Detailed scan parameters are listed in the On-line Table. All measurements were performed in the same session without interrupting the flow in the phantom.

Healthy Subjects

Fifteen healthy subjects (9 men/6 women; mean age, 25.4 ± 1.2 years) were included in the study. Ethical approval was obtained at the Regional Ethical Review Board in Lund, Sweden, or waived by the local ethics committee of the Amsterdam University Medical Centers, University of Amsterdam, Amsterdam, the Netherlands. Written informed consent was provided by all subjects.

After scout scans to locate the intracranial arteries in the circle of Willis, five blocks of flow MR imaging scans were performed in a randomized order per subject: 1) SENSE 4D flow, 2) PROUD 4D flow, 3) PROUD 4D flow rescan, 4) 2D flow, and 5) 2D flow rescan. The 4D flow scans (spatial resolution, 0.5 mm isotropic) were placed in a transversal plane to include the greatest possible part of the vasculature. The 2D flow scans were placed in a sagittal plane orthogonal to both left and right middle cerebral arteries and were considered as the reference for flow measurements (spatial resolution, 0.5 × 0.5 × 3.0 mm³; mean temporal resolution, 31.3 ± 0.6 ms; N_{card}, 30). The PROUD 4D flow scans were reconstructed with three different numbers of cardiac frames ($N_{card} = 7, 15, 30$), resulting in different mean temporal resolutions (134.0 ± 2.7 ms, 62.6 ± 1.2 ms, 31.3 ± 0.6 ms) and mean acceleration factors R = 5.7 ± 0.1, 10.6 ± 0.2, 19.9 ± 0.3, respectively. The SENSE 4D flow

scans were reconstructed into 7 cardiac frames. Detailed scan parameters are shown in the On-line Table.

Patients with Unruptured Intracranial Aneurysms

Five patients with UIAs (2 men/3 women; mean age, 63.1 ± 3.6 years) were scanned. Subjects provided written informed consent before the start of the study, which was approved by the local ethics committee of the Amsterdam University Medical Centers, University of Amsterdam, Amsterdam, the Netherlands.

A PROUD 4D flow scan was added to the examination protocol with a scan time of around 10 minutes. These scans were reconstructed with $N_{card} = 10$, 30 and $R = 9.9 \pm 0.2$, 26.1 ± 0.6, respectively (spatial resolution, 0.5 mm isotropic; mean temporal resolution, 94.7 ± 3.6 and 31.6 ± 1.2 ms). Detailed scan parameters are shown in the On-line Table.

Flow Analysis

Quantitative flow analysis was performed using Segment,[18] Version 2.2 (Medviso; http://medviso.com/).

Flow Phantom. All 4D flow MR imaging scans were resliced to the positions of the three 2D flow MR imaging scans (outlet, inlet right, and inlet left). A ROI was drawn on the cross-section of each tube, and these ROIs were copied to all datasets. Background phase correction was performed by defining a donut-shaped region as static tissue around the actual ROI. 4D flow scans were compared with the 2D flow scans, and mean differences over the three ROIs were measured of the peak flow rate, systolic stroke volume, and diastolic flow rate standard error. The systolic part (half of a cardiac cycle) was used for flow quantification, and the diastolic part for diastolic flow rate standard error calculation.

The 2D flow MR imaging scans were analyzed for repeatability by comparing the scan and rescan values.

Healthy Subjects. All 4D flow MR imaging scans were resliced to the positions of the two 2D flow MR imaging scans. ROIs were drawn on the cross-section of both MCAs in every dataset. Background phase correction was performed as in the flow phantom experiment. The first 4D flow MR imaging scans were compared with the first 2D flow MR imaging scan in peak flow rate, stroke volume, and the pulsatility index. The pulsatility index was calculated as the difference between the cross-sectional mean velocities at systole/maximum and diastole/minimum velocity divided by the mean velocity over the cardiac cycle.[19] Repeatability of the 2D flow MR imaging scan and the PROUD 4D flow MR imaging scan was analyzed by comparing the scan/rescan variability.

Patients with UIAs. The PROUD 4D flow MR imaging scans were postprocessed into a phase-contrast MRA,[20] which was used with the magnitude images to segment the intracranial vasculature and the aneurysms. WSS was calculated using in-house-developed software[21] in Matlab R2016a by multiplying the wall shear rate by the dynamic viscosity of blood (3.2×10^{-3} Pa·s). We performed two types of WSS calculations: WSS calculated at peak systole (WSS_{PS}) and time-averaged WSS (WSS_{TA}), in which the WSS is expressed as the average over the cardiac cycle. The WSS_{TA}, WSS_{PS}, and OSI were calculated for five patients with UIAs and expressed as the
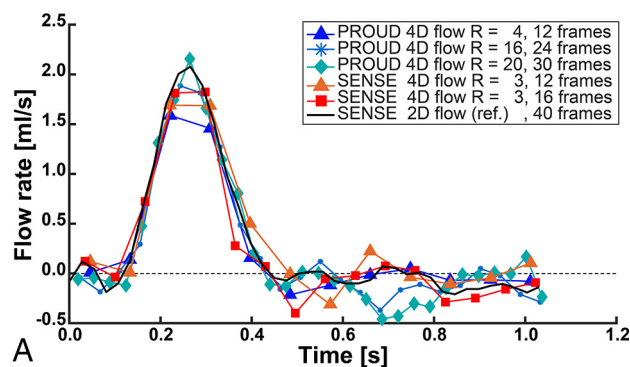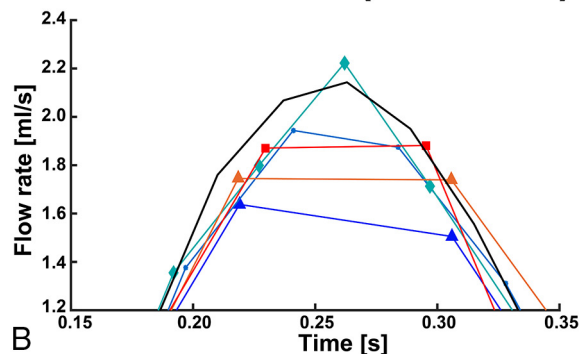

FIG 1. *A,* Flow rates of the outlet ROI of exemplary low (12 frames), moderate (16–24 frames), and high temporal resolution (30–40 frames). *B,* Zoomed view into the peak flow rate of the outlet ROI.

spatial mean value over the two ROIs: UIA only or surrounding vessel. Streamline flow visualizations of the aneurysms were made in GTFlow, Version 3.2.4 (GyroTools).

Statistical Analysis. Differences between two flow scans (A and B) were tested by orthogonal regression analysis and Spearman rank ρ as well as Bland-Altman plots (X = A, Y = A-B). Bland-Altman results were presented as the bias or mean difference $\pm$ standard error of the mean and limits of agreement. A Wilcoxon signed rank test was used for statistical evaluations with a $P < .05$ level of significance.

RESULTS
Flow Phantom

Flow phantom measurements showed good accuracy even at high acceleration factors (peak flow rate difference, <10%). The best trade-off between acceleration and flow rate error was obtained for R = 20–30 and $N_{card} \geq 30$. For a small peak flow rate error, at least 30 cardiac frames were needed.

Flow rates measured at the outlet ROI for low, moderate, and high temporal resolution are depicted in Fig 1. The differences between 2D flow and 4D flow MR imaging (2D flow – 4D flow) over all ROIs and scan sequences are listed in Table 1, and more flow rates are shown in On-line Fig 2.

Compared with 2D flow MR imaging, PROUD 4D flow MR imaging with $N_{card} \geq 30$ showed the smallest peak flow rate

Table 1: Results of the flow phantom analysis in terms of peak flow rate difference, stroke volume difference, and the SD of the diastolic flow

Sequence	Acceleration Factor	Cardiac Frames	Mean Peak Flow Rate Difference (mL/s) (%)	Mean Stroke Volume Difference (mL) (%)	Mean Diastolic Flow Rate SE (mL/s)
4D PROUD-1	32	12	−0.65 (−46.7%)	−0.036 (−15.3%)	0.028
4D PROUD-2	24	12	−0.52 (−35.0%)	−0.024 (−5.3%)	0.018
4D PROUD-3	16	12	−0.47 (−32.9%)	−0.040 (−14.3%)	0.033
4D PROUD-5	8	12	−0.45 (−31.6%)	−0.031 (−9.4%)	0.035
4D PROUD-4	12	12	−0.36 (−25.5%)	−0.024 (−7.4%)	0.021
4D PROUD-6	4	12	−0.34 (−23.9%)	−0.027 (−10.4%)	0.027
4D SENSE-1	3	12	−0.31 (−22.5%)	−0.007 (−5.2%)	0.047
4D SENSE-2	3	16	−0.27 (−21.5%)	−0.027 (−11.5%)	0.031
4D PROUD-5	16	24	−0.19 (−15.0%)	−0.002 (−3.2%)	0.029
4D PROUD-3	32	24	−0.18 (−13.5%)	−0.013 (−3.7%)	0.029
4D PROUD-6	8	24	−0.17 (−10.4%)	−0.028 (−10.6%)	0.024
4D PROUD-6	24	24	−0.13 (−8.0%)	−0.008 (−0.8%)	0.028
4D PROUD-5	26	40	−0.08 (−8.8%)	−0.011 (−2.0%)	0.027
4D PROUD-4	30	30	−0.06 (−7.8%)	0.005 (−3.3%)	0.022
4D PROUD-6	10	30	0.05 (1.9%)	−0.029 (−12.4%)	0.027
4D PROUD-6	13	40	−0.04 (−2.4%)	−0.031 (−11.4%)	0.024
4D PROUD-5	20	30	−0.03 (−4.3%)	0.003 (−4.9%)	0.034
2D reference-2	2	40	−0.05 (−3.7%)	−0.006 (−3.0%)	0.010
2D reference-1[a]	2	40	0.00 (0.0%)	0.000 (−0.0%)	0.011

Note:—SE indicates standard error.
[a] Used as a comparison baseline.

Table 2: Results of the healthy subject analysis in terms of peak flow rate difference, peak flow rate repeatability, stroke volume difference, stroke volume repeatability, and pulsatility index difference

	Comparison Pairs		Bland-Altman			Orthogonal Regression	
	A (Frames)	B (Frames)	Bias	LoA	P	Equation	ρ
Peak flow rate difference (mL/s)	2D reference-1 (30)	4D PROUD-1 (30)	0.31 ± 0.13	1.41	.22	y = 1.14x − 0.80	0.67
	2D reference-1 (30)	4D PROUD-1 (15)	0.51 ± 0.13	1.44	.03	y = 1.15x − 1.04	0.66
	2D reference-1 (30)	4D PROUD-1 (7)	0.76 ± 0.13	1.44	<.01	y = 0.90x − 0.42	0.60
	2D reference-1 (30)	4D SENSE (7)	0.79 ± 0.17	1.81	.01	y = 0.83x − 0.19	0.36
Peak flow rate repeatability (mL/s)	4D PROUD-1 (30)	4D PROUD-2 (30)	0.14 ± 0.08	0.90	.61	y = 0.87x + 0.28	0.87
	4D PROUD-1 (15)	4D PROUD-2 (15)	0.12 ± 0.08	0.87	.90	y = 0.84x + 0.37	0.88
	4D PROUD-1 (7)	4D PROUD-2 (7)	0.09 ± 0.07	0.71	.77	y = 0.90x + 0.17	0.89
	2D reference-1 (30)	2D reference-2 (30)	0.19 ± 0.08	0.86	.38	y = 1.01x − 0.23	0.86
Stroke volume difference (mL)	2D reference-1 (30)	4D PROUD-1 (30)	0.11 ± 0.09	0.94	.53	y = 0.99x − 0.08	0.64
	2D reference-1 (30)	4D PROUD-1 (15)	0.11 ± 0.09	0.94	.45	y = 0.97x − 0.04	0.64
	2D reference-1 (30)	4D PROUD-1 (7)	0.14 ± 0.09	0.93	.36	y = 0.95x − 0.03	0.64
	2D reference-1 (30)	4D SENSE (7)	0.15 ± 0.11	1.18	.36	y = 1.06x − 0.29	0.46
Stroke volume repeatability (mL)	4D PROUD-1 (30)	4D PROUD-2 (30)	0.08 ± 0.04	0.43	.57	y = 0.98x − 0.05	0.93
	4D PROUD-1 (15)	4D PROUD-2 (15)	0.08 ± 0.04	0.42	.60	y = 0.98x − 0.04	0.92
	4D PROUD-1 (7)	4D PROUD-2 (7)	0.07 ± 0.04	0.44	.64	y = 1.00x − 0.08	0.92
	2D reference-1 (30)	2D reference-2 (30)	0.06 ± 0.04	0.47	.80	y = 1.10x − 0.28	0.92
Pulsatility index difference (a.u.)	2D reference-1 (30)	4D PROUD-1 (30)	0.01 ± 0.04	0.39	.41	y = 1.97x − 0.82	0.15
	2D reference-1 (30)	4D PROUD-1 (15)	0.18 ± 0.04	0.39	<.01	y = 1.51x − 0.60	0.10
	2D reference-1 (30)	4D PROUD-1 (7)	0.31 ± 0.03	0.33	<.01	y = 0.01x + 0.51	0.01
	2D reference-1 (30)	4D SENSE (7)	0.31 ± 0.03	0.35	<.01	y = 0.03x + 0.50	0.02

Note:—LoA indicates limits of agreement; a.u., arbitrary units.

underestimation. Furthermore, PROUD 4D flow MR imaging with N_{card} = 24 underestimated peak flow rate, comparable with conventional SENSE-accelerated 4D flow MR imaging. All PROUD 4D flow scans with N_{card} = 12 underestimated peak flow rate to a greater extent than 4D flow scans with N_{card} = 24. Stroke volume differences had no clear trend over the temporal resolutions, and the error was never higher than 15%. Diastolic flow rate standard error showed higher signal variation for the 4D flow than the 2D flow scans, but no clear trend with acceleration could be observed.

The 2D flow MR imaging repeatability analysis showed steady pump conditions (Bland-Altman: bias, 0.002 ± 0.007 mL/s; limits of agreement, 0.14 mL/s; regression, y = 0.98x + 0.00, ρ = 0.99).

Healthy Subjects

Flow measurements in healthy subjects showed good agreement between highly accelerated (R = 20) high temporal resolution 4D flow and 2D flow scans.

Examples of magnitude and phase images of the three 4D flow scans are shown in On-line Fig 3. Image quality was

comparable, but more blurring was visible for high acceleration, particularly in the magnitude images. Peak flow rate differences between 2D flow and 4D flow MR imaging are shown in Table 2 and On-line Fig 4. It can be seen that the flow rate difference decreased for higher temporal resolutions. For $N_{card} = 7, 15$, flow rate difference values were significantly different, but not for $N_{card} = 30$. Orthogonal regression analysis revealed an improved correlation between

UIA patient 5
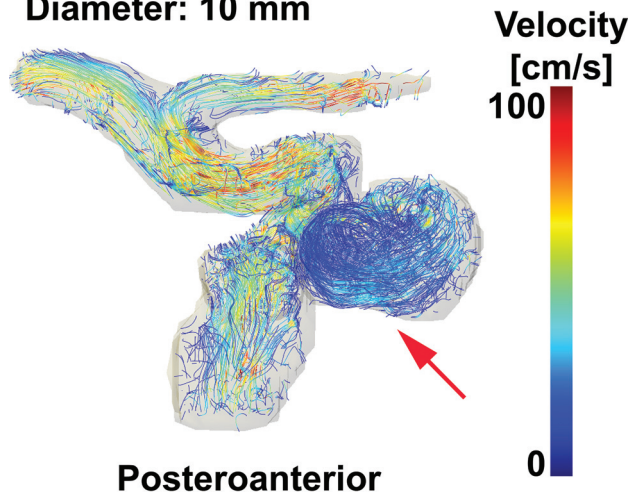## Location: MCA left
Diameter: 10 mm

FIG 2. Streamlines of patient 5 with an UIA to visualize blood flow patterns in the aneurysm (*red arrow*) of 10-mm diameter located at the left MCA. A video of streamlines of all five patients with UIAs over the cardiac cycle can be seen in the On-line Video. MCA indicates middle cerebral artery.

2D and 4D flow MR imaging when using a higher number of cardiac frames. Similar peak flow rate repeatability (bias and limits of agreement) was observed for PROUD 4D flow compared with the 2D flow scans (Table 2 and On-line Fig 5). No significant differences in stroke volumes were observed for the four 4D flow scans compared with the 2D flow scans (Table 2 and On-line Fig 6). The stroke volume in PROUD 4D flow and 2D flow scans also had similar repeatability (Table 2 and On-line Fig 7). Pulsatility index differences were significant for 4D flow MR imaging with $N_{card} = 7, 15$, compared with the 2D flow MR imaging, but not for 4D flow MR imaging with $N_{card} = 30$ (Table 2 and On-line Fig 8). However, the Spearman ρ did not indicate a high correlation for the pulsatility index between 2D flow and 4D flow MR imaging.

Patients with UIAs
The 4D flow MR imaging scans in the patients with UIAs showed a trend toward higher OSI for increased temporal resolution, but a similar trend could not be found in the WSS of all aneurysms.

Vortices were seen in the streamline visualizations for patients 1, 4, and 5 (Fig 2), but not for patients 2 and 3. Streamlines over the cardiac cycle of all patients are visualized in the On-line Video. Visualizations of WSS_{TA}, WSS_{PS}, and OSI of patient 5 for $N_{card} = 10, 30$ are shown in Fig 3. With increased temporal resolution, the WSS_{PS} and the OSI increased as well in some areas of the aneurysm wall. In Fig 4, the mean values of WSS_{TA}, WSS_{PS}, and OSI per UIA are presented as well as the mean values of WSS_{TA} and WSS_{PS} of their in- and outflow vessels. In the UIAs of patients 2 and 5 as well as in the vessel in all patients, WSS_{PS} was higher than WSS_{TA}, regardless of the temporal resolution. In the UIAs of patients 3 and 5, WSS_{TA} and WSS_{PS} were higher for $N_{card} = 30$ than for $N_{card} = 10$ frames. In the UIAs of
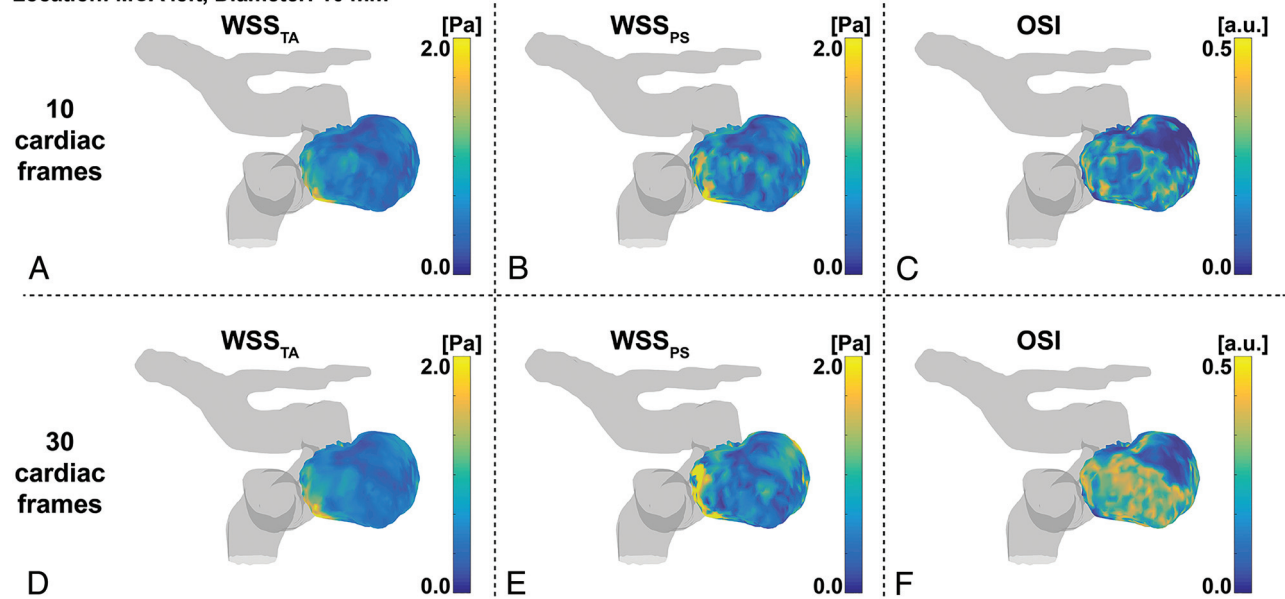

FIG 3. Example WSS and OSI analysis of patient 5. Time-averaged WSS on the left, peak-systolic WSS in the middle, and OSI on the right for datasets with either 10 (*upper row*) or 30 (*lower row*) cardiac frames. MCA indicates middle cerebral artery; a.u., arbitrary units.
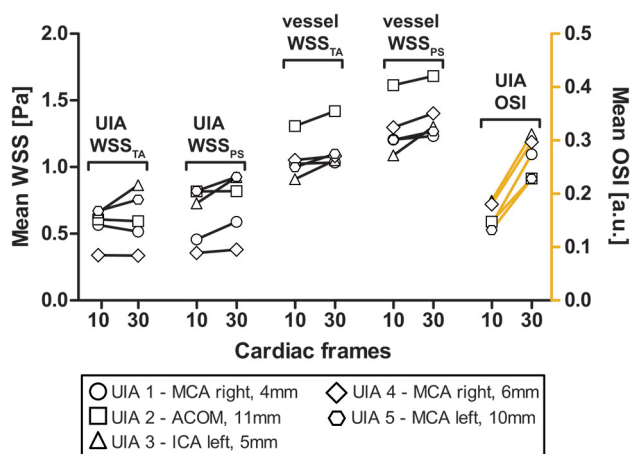
FIG 4. The changes in time-averaged WSS, peak systolic WSS, and OSI in the aneurysm and in the surrounding vessel when increasing the temporal resolution from 10 to 30 cardiac frames, or from 95 to 32 ms, respectively. ACOM indicates anterior communicating artery; ICA, internal carotid artery; MCA, middle cerebral artery; a.u., arbitrary units.

patients 1, 2, and 4, no clear difference or trend between the two temporal resolutions was observed. In all UIAs, the OSI was higher for $N_{card} = 30$ than for $N_{card} = 10$ frames.

DISCUSSION

This study investigated whether highly accelerated high resolution 4D flow MR imaging in intracranial arteries and aneurysms at 7T can provide reliable quantitative flow values in a clinically acceptable scan time of about 10 minutes using a pseudospiral Cartesian sampling scheme with CS reconstruction. Results showed that stroke volumes and peak flow rate values from 4D flow MR imaging, with $R = 20$–30 acceleration and a high temporal resolution of 30 cardiac frames, were similar to those obtained with 2D flow MR imaging.

Pulsatile flow phantom experiments were used to investigate the trade-off between scan acceleration and accuracy of flow measurements. The error in the peak flow rate decreased with an increasing number of cardiac frames, and stroke volume was underestimated in an acceptable level even for high temporal resolution ($<3\times$ difference of 2D rescan). The diastolic flow rate standard error in 4D flow scans showed 2–4 times larger variation than the 2D reference scans, and there was no clear trend observable for changes in acceleration or temporal resolution. Thus, we interpret this finding as acceptable random reconstruction- or undersampling-based artifacts. Taken together, we used $R = 30$ as maximum acceleration factor for the in vivo scans when reconstructing the data into 30 cardiac frames. In vivo measurements then confirmed that highly accelerated 4D flow MR imaging with a high temporal resolution resulted in small errors compared with 2D flow MR imaging. Furthermore, PROUD 4D flow MR imaging was superior to conventional 4D flow MR imaging, especially for those reconstructed in 30 cardiac frames, which resulted in the lowest peak flow rate difference. When we compared PROUD with conventional 4D flow MR imaging, the flow rate accuracy (peak flow rate difference to 2D

flow MR imaging) was increased by 60%, while both had the same scan duration.

Reduced scan time is important for patients, which is why high acceleration is needed. However, there are only a few reports on acceleration factors above 10, especially at 7T field strength. Comparable high acceleration is only reported for acquisition and reconstruction similar to methods used in this study, which all deal with large multidimensional datasets. Cheng et al[22] reported $R \approx 19$ for accelerated 4D flow MR imaging in the heart at 3T and also used temporal total variation in the reconstruction. Walheim et al[23] reported $R = 19$ for accelerated 5D flow MR imaging in the aorta at 3T. Rich et al[24] demonstrated 4D flow imaging of the aortic valve at 1.5T with acceleration up to a factor 27. Gu et al[25] also acquired 4D flow data in the intracranial arteries, but at 1.5T, and reported a usable acceleration up to a factor of 30.

Considering the aneurysm and surrounding intracranial vasculature, two main observations could be made from the derived WSS. First, WSS_{PS} and WSS_{TA} as well as OSI in the vessels were higher with increased temporal resolution. Second, WSS_{PS} was higher than WSS_{TA} regardless of the temporal resolution. These two observations can be explained by the increased peak flow rate accuracy observed in the phantom experiment and healthy subjects. Measured WSS in the aneurysms was lower than in the surrounding intracranial vasculature, which is in line with previous results.[26] Increased temporal resolution resulted in increased OSI in all aneurysms, which has also been reported previously.[12] Most interesting, increased temporal resolution resulted in increased WSS in only two aneurysms but rather constant WSS in three aneurysms. Moreover, WSS_{PS} was higher than WSS_{TA} in only two aneurysms. Thus, we did not observe a clear trend for the WSS in the aneurysms. A likely explanation can be found in the differences in size and geometry of the aneurysms; for a UIA with low and constant flow, the improved temporal resolution will not change WSS estimations.[26] For cases of complex flow patterns, this finding suggests that flow and WSS estimations in aneurysms will benefit from the improved temporal resolution provided by our accelerated protocols. We will pursue studies in larger cohorts of patients to further investigate the added value of high temporal resolution WSS in aneurysm rupture risk predictions.

Previous studies on WSS do not agree on which WSS calculation method should be used,[4,13,26-28] but temporal fluctuations in WSS were associated with aneurysm risk of growth or formation.[11,27] Thus, indicators like the OSI[11] or the aneurysm formation indicator[27] were developed to express these temporal fluctuations in WSS. Most of these models use a reference vector, commonly the time-averaged WSS vector, based on the assumption that the endothelial cells are preferentially aligned in the direction of this vector.[27] When one uses these metrics, it is likely that a higher temporal resolution will give a more accurate outcome of temporal fluctuations in WSS.

A possible key application for high temporal resolution 4D flow MR imaging data is the combination of 4D flow MR imaging with computational fluid dynamics simulations, which have been shown to be a useful clinical tool for the prediction of the

initiation, growth, and rupture of aneurysms.[13,26] Prior research combining fluid dynamics and 4D flow showed better agreement than calculations alone.[4,29] MR imaging–guided computational fluid dynamics can be used to correct the MR imaging–measured flow field, forcing it to satisfy the fluid mechanics equations. It can also be used as a means of reducing imperfections in the 4D flow MR imaging measurements and may improve the ability to accurately derive clinically relevant secondary parameters such as WSS and pressure gradients at a much higher level of detail and confidence than was previously possible.[29,30]

Because highly accelerated 4D flow MR imaging with high temporal resolution provided reliable quantitative flow values, we encourage using 4D flow MR imaging more often for UIA monitoring and growth prediction in future clinically focused studies.[6,26] The techniques must be investigated in a larger study of patients with UIAs to determine whether the derived WSS is affected by either the calculation method or the temporal resolution or both. If it turns out that high temporal resolution does not add any value for clinical outcome, then the acceleration of the 4D flow MR imaging scan can be used to improve coverage and resolution or to further shorten the scan duration. Eventually, a consensus on 4D flow MR imaging followed by WSS calculation and analysis for intracranial aneurysm is desirable.

Limitations

A more complex phantom could mimic the intracranial arteries and their flow distribution better. Moreover, a pump with combined systolic pulsatile and diastolic steady flow could reduce the signal variation during the diastolic period. Furthermore, temporal fluctuations in WSS or OSI are sensitive to deviations induced by high acceleration. This limitation might be reduced when combining 4D flow MR imaging with computational fluid dynamics, which performs well in de-noising and preserving details in the velocity profiles. Finally, the study population to investigate the effect of increased temporal resolution for WSS calculations in patients with UIAs was too small to draw a significant conclusion.

CONCLUSIONS

Highly accelerated high spatiotemporal resolution 4D flow MR imaging in intracranial arteries and aneurysms at 7T provides repeatable quantitative flow values in a clinically acceptable scan time of ~10 minutes, using pseudospiral Cartesian sampling with compressed sensing reconstruction. In vivo measurements showed that the accuracy of the flow rate was significantly increased compared with conventional low temporal resolution 4D flow scans. Data from patients with unruptured intracranial aneurysms show that the improved temporal resolution influences the oscillatory shear index.

ACKNOWLEDGMENT

We would like to thank Eva L. Leemans and Bart M.W. Cornelissen for the collection of the patient data, which was funded by the Stichting Toegepast Wetenschappelijk Instituut voor Neuromodulatie.

REFERENCES

1. Steiner T, Juvela S, Unterberg A, et al. **European stroke organization guidelines for the management of intracranial aneurysms and subarachnoid haemorrhage.** *Cerebrovasc Dis* 2013;35:93–112 CrossRef Medline
2. Thompson BG, Brown RD, Amin-Hanjani S, et al; American Heart Association Stroke Council, Council on Cardiovascular and Stroke Nursing, and Council on Epidemiology and Prevention; American Heart Association; American Stroke Association. **Guidelines for the management of patients with unruptured intracranial aneurysms.** *Stroke* 2015;46:2368–2400 CrossRef Medline
3. Markl M, Frydrychowicz A, Kozerke S, et al. **4D flow MRI.** *J Magn Reson Imaging* 2012;36:1015–36 CrossRef Medline
4. van Ooij P, Potters WV, Guédon A, et al. **Wall shear stress estimated with phase contrast MRI in an in vitro and in vivo intracranial aneurysm.** *J Magn Reson Imaging* 2013;38:876–84 CrossRef Medline
5. Coolen BF, Calcagno C, van Ooij P, et al. **Vessel wall characterization using quantitative MRI: what's in a number?** *MAGMA* 2018;31:201–22 CrossRef Medline
6. Boussel L, Rayz V, McCulloch C, et al. **Aneurysm growth occurs at region of low wall shear stress: patient-specific correlation of hemodynamics and growth in a longitudinal study.** *Stroke* 2008;39:2997–3002 CrossRef Medline
7. Chung BJ, Mut F, Putman CM, et al. **Identification of hostile hemodynamics and geometries of cerebral aneurysms: a case-control study.** *AJNR Am J Neuroradiol* 2018;39:1860–66 CrossRef Medline
8. Blankena R, Kleinloog R, Verweij BH, et al. **Thinner regions of intracranial aneurysm wall correlate with regions of higher wall shear stress: a 7T MRI study.** *AJNR Am J Neuroradiol* 2016;37:1310–17 CrossRef Medline
9. Cebral JR, Detmer F, Chung BJ, et al. **Local hemodynamic conditions associated with focal changes in the intracranial aneurysm wall.** *AJNR Am J Neuroradiol* 2019;40:510–16 CrossRef Medline
10. van Ooij P, Zwanenburg JJM, Visser F, et al. **Quantification and visualization of flow in the circle of Willis: time-resolved three-dimensional phase contrast MRI at 7 T compared with 3 T.** *Magn Reson Med* 2013;69:868–76 CrossRef Medline
11. Ku DN, Giddens DP, Phillips DJ, et al. **Hemodynamics of the normal human carotid bifurcation: in vitro and in vivo studies.** *Ultrasound Med Biol* 1985;11:13–26 Medline
12. Cibis M, Potters WV, Gijsen FJ, et al. **The effect of spatial and temporal resolution of cine phase contrast MRI on wall shear stress and oscillatory shear index assessment.** *PLoS One* 2016;11:e0163316–15 CrossRef Medline
13. Boussel L, Rayz V, Martin A, et al. **Phase-contrast magnetic resonance imaging measurements in intracranial aneurysms in vivo of flow patterns, velocity fields, and wall shear stress: comparison with computational fluid dynamics.** *Magn Reson Med* 2009;6:409–17 CrossRef Medline
14. Lustig M, Donoho D, Pauly JM. **Sparse MRI: The application of compressed sensing for rapid MR imaging.** *Magn Reson Med* 2007;58:1182–95 CrossRef Medline
15. Peper ES, Gottwald LM, Zhang Q, et al. **Highly accelerated 4D flow cardiovascular magnetic resonance using a pseudo-spiral Cartesian acquisition and compressed sensing reconstruction for carotid flow and wall shear stress.** *J Cardiovasc Magn Reson* 2020;22:7 CrossRef Medline
16. Gottwald LM, Peper ES, Zhang Q, et al. **Pseudo-spiral sampling and compressed sensing reconstruction provides flexibility of temporal resolution in accelerated aortic 4D flow MRI: a comparison with**

K-T principal component analysis. *NMR Biomed* 2020;33:e4255 CrossRef Medline

17. Uecker M, Ong F, Tamir JI, et al. **Berkeley advanced reconstruction toolbox.** *In: Proceedings of the International Society for Magnetic Resonance in Medicine*, May 30 to June 5, 2015; Toronto, Ontario, Canada; 2486

18. Heiberg E, Sjögren J, Ugander M, et al. **Design and validation of Segment: freely available software for cardiovascular image analysis.** *BMC Med Imaging* 2010;10:1 CrossRef Medline

19. Bouvy WH, Geurts LJ, Kuijf HJ, et al. **Assessment of blood flow velocity and pulsatility in cerebral perforating arteries with 7-T quantitative flow MRI.** *NMR Biomed* 2016;29:1295–1304 CrossRef Medline

20. Bock J, Frydrychowicz A, Stalder AF, et al. **4D phase contrast MRI at 3 T: effect of standard and blood-pool contrast agents on SNR, PC-MRA, and blood flow visualization.** *Magn Reson Med* 2010;63:330–38 CrossRef Medline

21. Potters WV, van Ooij P, Marquering H, et al. **Volumetric arterial wall shear stress calculation based on cine phase contrast MRI.** *J Magn Reson Imaging* 2015;41:505–16 CrossRef Medline

22. Cheng JY, Hanneman K, Zhang T, et al. **Comprehensive motion-compensated highly accelerated 4D flow MRI with ferumoxytol enhancement for pediatric congenital heart disease.** *J Magn Reson Imaging* 2016;43:1355–68 CrossRef Medline

23. Walheim J, Dillinger H, Kozerke S. **Multipoint 5D flow cardiovascular magnetic resonance - accelerated cardiac- and respiratory-motion resolved mapping of mean and turbulent velocities.** *J Cardiovasc Magn Reson* 2019;21:42 CrossRef Medline

24. Rich A, Potter LC, Jin N, et al. **A Bayesian model for highly accelerated phase-contrast MRI.** *Magn Reson Med* 2016;76:689–701 CrossRef Medline

25. Gu T, Korosec FR, Block WF, et al. **PC VIPR: a high-speed 3D phase-contrast method for flow quantification and high-resolution angiography.** *AJNR Am J Neuroradiol* 2005;26:743–49 Medline

26. Shojima M, Oshima M, Takagi K, et al. **Magnitude and role of wall shear stress on cerebral aneurysm: computational fluid dynamic study of 20 middle cerebral artery aneurysms.** *Stroke* 2004;35:2500–05 CrossRef Medline

27. Mantha A, Karmonik C, Benndorf G, et al. **Hemodynamics in a cerebral artery before and after the formation of an aneurysm.** *AJNR Am J Neuroradiol* 2006;27:1113–18 Medline

28. Schnell S, Wu C, Ansari SA. **Four-dimensional MRI flow examinations in cerebral and extracerebral vessels: ready for clinical routine?** *Curr Opin Neurol* 2016;29:19–28 CrossRef Medline

29. Töger J, Zahr MJ, Aristokleous N, et al. **Blood flow imaging by optimal matching of computational fluid dynamics to 4D-flow data.** *Magn Reson Med* 2020 Apr 8. [Epub ahead of print] CrossRef Medline

30. Bakhshinejad A, Baghaie A, Vali A, et al. **Merging computational fluid dynamics and 4D-Flow MRI using proper orthogonal decomposition and ridge regression.** *J Biomech* 2017;58:162–73 CrossRef Medline